

An MRI-Derived Definition of MCI-to-AD Conversion for Long-Term, Automatic Prognosis of MCI Patients for the Alzheimer’s Disease Neuroimaging Initiative[☆]

Yaman Aksu^a, David J. Miller^b, George Kesidis^{b,c}, Don C. Bigler^d, Qing X. Yang^a

^a*Center for NMR Research, Department of Radiology, Penn State University College of Medicine, Hershey, PA, USA*

^b*Electrical Engineering Department, Penn State University, University Park, PA, USA*

^c*Computer Science and Engineering Department, Penn State University, University Park, PA, USA*

^d*Center for Emerging Neurotechnology and Imaging, Penn State University College of Medicine, Hershey, PA, USA*

Abstract

Alzheimer’s disease (AD), and its precursor state, mild cognitive impairment (MCI), continue to be widely studied. While there is no consensus on whether MCIs actually “convert” to AD, this *concept* is widely applied, allowing statistical testing and machine learning methods to help identify early disease biomarkers and build models for predicting disease progression. Thus, the more important question is not *whether* MCIs convert, but *what is the best such definition*. We focus on automatic prognostication, nominally using only a baseline image brain scan, of whether an MCI individual will convert to AD within a multi-year period following the initial clinical visit. This is in fact not a traditional supervised learning problem since, in ADNI, *there are no definitive labeled examples of MCI conversion*. It is not truly unsupervised, either, since there are (labeled) AD and Control subjects, as well as clinical and cognitive scores for MCIs. Prior works have defined MCI subclasses

[☆]Data used in preparation of this article were obtained from the Alzheimer’s Disease Neuroimaging Initiative (ADNI) database (adni.loni.ucla.edu). As such, the investigators within the ADNI contributed to the design and implementation of ADNI and/or provided data but did not participate in analysis or writing of this report. A complete listing of ADNI investigators can be found at: http://adni.loni.ucla.edu/wp-content/uploads/how_to_apply/ADNI_Authorship_List.pdf

based on whether or not clinical/cognitive scores significantly change from baseline. There are serious concerns with these definitions, however, since e.g. most MCIs (*and ADs*) do not change from a baseline CDR=0.5 at any subsequent visit in ADNI, even while physiological changes may be occurring. These works ignore rich *phenotypical* information in an MCI patient’s brain scan and labeled AD and Control examples, in defining conversion. We propose an innovative conversion definition, wherein an MCI patient is declared to be a converter if any of the patient’s brain scans (at follow-up visits) are classified “AD” by an (accurately-designed) Control-AD classifier. This novel definition *bootstraps* the design of a *second* classifier, *specifically trained to predict whether or not MCIs will convert*. This second classifier thus predicts whether an AD-Control classifier will predict that a patient has AD. Our results demonstrate this new definition leads not only to much higher prognostic accuracy than by-CDR conversion, but also to subpopulations much more consistent with *known* AD brain region biomarkers. We also identify key *prognostic* region biomarkers, essential for accurately discriminating the converter and nonconverter groups.

Keywords: Alzheimer’s, mild cognitive impairment, AD conversion, MRI, support vector machines, feature selection, AD biomarkers, MFE, RFE

1. Introduction

The dementing illness Alzheimer’s disease (AD), and the transitional state between normal aging and AD referred to as mild cognitive impairment (MCI) continue to be widely studied. Individuals diagnosed with MCI have memory impairment, yet without meeting dementia criteria. Annually $\approx 10\text{-}15\%$ of people with MCI are diagnosed with AD (Petersen, 2004). Moreover, prior to symptom onset, brain abnormalities have been found in people with MCI, as ascertained by retroactive evaluation of longitudinal MRI scans (Davatzikos et al., 2008). There is no consensus on whether MCI patients actually “convert” to AD. First, some MCI patients may suffer from other neurodegenerative disorders (e.g., Lewy body dementia, vascular dementia and/or frontotemporal dementia). Second, it is possible that all other MCI patients already have AD, but at a preclinical stage. AD diagnosis itself may not be considered definitive without e.g. confirming pathologies such as the amyloid deposits detectable at autopsy. Regardless of whether MCI patients truly “convert” to AD or not, the concept of MCI-to-AD conversion has been

widely applied, e.g. (Chou et al., 2009; Davatzikos et al., 2010; Misra et al., 2009; Vemuri et al., 2009; Zhang et al., 2011) and is utilitarian – defining MCI (converter and nonconverter) subgroups allows use of statistical group difference tests and machine learning methods to help identify early disease biomarkers and to build models for predicting disease progression. For these purposes, the more important question is not whether MCIs convert, but rather *what is the best such definition*.

Accordingly, here we focus on the following **Aim**: automatic prognostication, (nominally) using only a baseline brain scan, of whether an MCI individual will convert to AD within a multi-year (three year) period following an initial (baseline) clinical visit¹.

While only image voxel-based features are evaluated here for use by our classifier, our framework is extensible to incorporating other baseline clinical information (e.g. weight, gender, education level, genetic information, and clinical cognitive scores such as the Mini Mental State Exam (MMSE)) into the decisionmaking. Moreover, our approach can also incorporate the recent, promising cerebrospinal fluid (CSF) based markers (De Meyer et al., 2010). However, as this requires an invasive spinal tap, we focus here on image scans, which are routinely performed for subjects with MCI.

We do not hypothesize that, within ADNI, there are actually two subclasses of MCI subjects when evaluated over the very long term – those that (eventually) convert to AD, and those that do not. Even if an overwhelming majority of MCI subjects will *eventually* convert, identifying the subgroup likely to convert *within several years* has several compelling utilities: 1) early prognosis, to assist family planning; 2) facilitating group-targeted treatments/drug trials; 3) we identify key *prognostic* brain “biomarker” regions, *i.e.* those found to be most critical for accurately discriminating our “converter” and “nonconverter” groups. These regions may shed light on disease etiology.

Distinguishing AD converters from nonconverters is a binary (two-class) classification problem. Moreover, it may appear this classification problem can be directly addressed via supervised learning methods (Duda et al., 2001). However, it is in fact an *unconventional* problem, lying somewhere *between* supervised classification and unsupervised classification (clustering), and thus

¹Our system performs three-year ahead prediction because it is designed based on the ADNI database, which followed participants for a period of up to three years.

requiring a unique approach. To appreciate this, consider the ADNI cohort of MCI individuals. ADNI consists of clinical information and image scans on hundreds of participants, taken at six-month intervals for up to three years. A clinical label (AD, MCI, or Control) was assigned to each participant at first visit². Even though a *probable AD* definition based on CDR and MMSE scores and NINCDS/ADRDA criteria has been used, e.g. (Leow et al., 2009; Zhang et al., 2011), to provide follow-up assessment for MCI patients, this is strictly a clinically driven definition, based on a clinical rating (CDR) and a cognitive score (MMSE) whose difficulties will be pointed out shortly. This is not a definitive (autopsy-based) determination of AD, nor is it a definition based on physiological brain changes. Even if the *probable AD* definition has very high *specificity*, it may not be sufficiently sensitive, i.e. there may be patients who are undergoing significant physiological brain changes consistent with conversion, yet without clinical manifestation.

Accordingly, we will approach the conversion problem from a perspective as agnostic and unbiased as possible, and simply state that it is not definitively known which MCI participants in ADNI truly converted to AD within three years. In conventional supervised classifier learning, one has labeled training examples, used for designing the classifier, and labeled test examples, used to estimate the classifier’s generalization accuracy. For predicting whether MCI participants in ADNI convert to AD, we in fact have neither. Thus, our problem is not conventional supervised learning. On the other hand, consider *unsupervised* clustering (Duda et al., 2001). Here, even if one knows the number of clusters (classes) present, there is no prior knowledge on what is a good clustering – one is simply looking for underlying grouping tendency in the data. Clearly, our problem does not fit unsupervised clustering, either – while we have no labeled MCI converter/nonconverter instances per se, 1) there are two designated classes of interest (converter and nonconverter); and 2) there are known class characteristics – conversion to AD should, plausibly, mean that: (i) a clinical measure such as CDR or a cognitive measure has changed *and/or* (ii) there are changes in brain features more characteristic of AD subjects than normal/healthy subjects. Note that in ADNI we do have plentiful labeled AD and normal/healthy (Control)

²Clinicians derive the AD/MCI/Control label based on multiple criteria, which may include Clinical Dementia Rating (CDR), whose possible values are: $0=none$, $0.5=questionable$, $1=mild$, $2=moderate$, $3=severe$.

examples to help assess ii).

Based on the above, MCI prognosis is an interesting and novel problem, lying somewhere between supervised and unsupervised classification. The crux of this problem is to craft criteria through which meaningful MCI subgroups can be defined, well-capturing notions of “AD converter” and “non-converter”. To help guide development and evaluation of candidate definitions, we state the following three **desiderata**: 1) The proposed definition of AD converter should be plausible and should exploit the available, relevant information in the ADNI database (e.g. image data, labeled AD and Control examples, and clinical information). To appreciate 1), note that the MCI population could be dichotomized in *many* ways, e.g. by height, and there might be significant clustering tendency with respect to height, but such a grouping is likely meaningless for MCI prognosis; 2) A classifier trained based on these class definitions should *generalize* well on test data (not used for training the classifier) – this quantifies how accurately we can discriminate the classes that we have defined. If we create what we believe to be good definitions, but ones that cannot be accurately discriminated, that would not be useful clinically; 3) The class definitions should be validated using known AD conversion biomarkers (*i.e.*, external measures) such as measured changes from baseline both in volumes of brain regions known to be associated with the disease (Schuff et al., 2010) and in cognitive test scores (such as the clinical MMSE measure).

Prior Related Work

Several prior works, e.g. (Davatzikos et al., 2010; Misra et al., 2009; Wang et al., 2010), defined converter and nonconverter classes *solely* according to whether the baseline visit CDR score of 0.5 rose or stayed the same over all visits. Change in CDR has also been used as surrogate ground-truth for cognitive decline in a number of other papers, e.g. (Chou et al., 2010; Vemuri et al., 2009). While CDR gives a workable conversion definition, it should be evaluated with respect to the three desiderata above. We will evaluate 2) and 3) in the sequel. With respect to 1), one should challenge a CDR-based conversion definition. First, CDR is not an effective discriminator between the AD and MCI groups, *i.e.* there is *very significant* AD-MCI overlap, not only with respect to CDR=1 *but even 0.5* – for ADNI, the majority of the hundreds of AD subjects used in our experiments start (at first visit) at CDR=0.5 and stay at 0.5 at *all* later visits; likewise, nearly all MCI subjects start at 0.5, with a large majority of these *also* staying at 0.5 for all visits. This latter fact further implies difficulties in finding an adequate

number of conversion-by-CDR subjects in ADNI, both for accurate classifier training and test set evaluation. For the even more stringent *probable AD* definition (meeting MMSE and NINCDS/ADRDA criteria, in addition to CDR changing from 0.5 to 1) there are necessarily even *fewer* MCI converters for classifier training and testing. Second, a purely CDR-based (or “probable AD” based) conversion definition ignores the (rich) *phenotypical* information in an MCI subject’s image brain scans and does not exploit the labeled AD and normal/healthy (Control) examples in ADNI. These prior works do treat features derived from brain scans as the *covariates* (the inputs) to the classifier/predictor. However, we believe the MCI brain scans can themselves be used, in conjunction with the labeled AD and Control examples, to help define more accurate surrogate ground-truth.

Previous work has demonstrated that structural MRI analysis is useful for identifying AD biomarkers in individual brain regions (Chetelat et al., 2002; Fan et al., 2008; Fennema-Notestine et al., 2009) – *e.g.*, cortical thinning (Lerch et al., 2005; Thompson et al., 2003), ventricle dilation and gaping (Chou et al., 2010, 2009; Schott et al., 2005), volumetric and shape changes in the hippocampus and entorhinal cortex (Csernansky et al., 2005; de Leon et al., 2006; Stoub et al., 2005), and temporal lobe shrinkage (Rusinek et al., 2004). It is important to capture interaction effects across multiple brain regions. (Davatzikos et al., 2008; Misra et al., 2009; Vemuri et al., 2008; Wang et al., 2010) did jointly analyze voxels (or regions) spanning the entire brain and did build classifiers or predictors. Moreover, as part of their work, (Wang et al., 2010) investigated prediction of future decline in MCI subjects working from baseline MRI scans, which is the primary subject of our current paper. However, there are several limitations of these past works. First, all these studies used the previously discussed CDR and cognitive measures such as MMSE, which has been described as noisy and unreliable, as the ground-truth prediction targets for classifier/regressor training. In (Chou et al., 2010), the authors state: “Cognitive assessments are notoriously variable over time, and there is increasing evidence that neuroimaging may provide accurate, reproducible measures of brain atrophy.” Even in (Wang et al., 2010), where MMSE was treated as the measure of decline and the ground-truth regression target, the authors acknowledged that “individual cognitive evaluations are known to be extremely unstable and depend on a number of factors unrelated to...brain pathology.” Such factors include sleep deprivation, depression, other medical conditions, and medications. Even though MMSE is widely used by clinicians, these comments (even if not universally

accepted), do indicate MMSE by itself may not be so reliable in quantifying the disease state. Moreover, while (Wang et al., 2010) did build predictors of future MMSE scores working from baseline scans, this was not a main focus of their paper – their paper focused on predicting the current score. Their prognostic experiments involved a very small sample size (just 26 participants from the ADNI database). Accordingly, it is difficult to draw definitive conclusions about the accuracy of their prognostic model and their associated brain biomarkers. The main reason the authors chose such a small sample was, as the authors state: “A large part of...ADNI...are from patients who did not display significant cognitive decline...[these] would overwhelm the regression algorithm if..used in the...experiment.” While this statement (with cognitive decline measured according to MMSE) may be true, that does not mean many of those excluded ADNI subjects are not experiencing significant physiological brain changes/atrophy. The novel approach we next sketch is well-suited to identifying MCI subjects undergoing such changes.

Our Neuroimaging-Driven, Trajectory-Based Approach

Here, we propose a novel approach for prognosticating putative conversion to AD driven by image-based information (and exploiting AD-Control examples), rather than by a single, non-image-based, weakly discriminating clinical measurement such as CDR. Our solution strategy is as follows. We first build an accurate image-based Control-AD classifier (*i.e.*, using AD and Control subjects, we build a Support Vector Machine (SVM) classifier) (Vapnik, 1998). We then apply this classifier to a *training population* of MCI subjects – separately, for each subject visit, we determine whether the subject’s image is on the AD side or the Control side of the SVM’s fixed (hyperplane) decision boundary. In addition to a binary decision, the SVM gives a “score” – essentially the distance to the classifier’s decision boundary. Thus, for each MCI subject, as a function of visits, we get an image-based “phenotypical” score trajectory. We fit a line to each subject’s trajectory and extend the line to the sixth visit if the sixth visit is missing. We can then give the following *trajectory-based conversion definition*: if the extended line either starts on the AD side or crosses to the AD side over the six visits, we declare this person a “converter-by-trajectory”. Otherwise, this person is a “nonconverter-by-trajectory”³. In this fashion, we *derive* ground-truth

³A very small percentage of the MCI population, in our experiments often 1% and not exceeding 5%, may unexpectedly start on the AD side and cross to the Control side. We

“converter” and “nonconverter” labels for an (initially unlabeled) training MCI population. These (now) labeled training samples *bootstrap* the design of a *second* SVM classifier which uses only the first-visit training set MCI images and is trained to predict whether or not an MCI patient is a “converter-by-trajectory”. Essentially, this second (prognostic) classifier is predicting whether, within three years, an AD-Control classifier will predict that a patient has AD. Via these two classifier design steps, we thus build a classification system for our (unconventional) pattern recognition task.

SVMs are widely used classifiers whose accuracy is attributed to their maximization of the “margin”, *i.e.* the smallest distance from any training point to the classification boundary. Since the SVM finds a linear discriminant function that *maximizes* margin, a significant change in score is generally needed to cross from the control side to the AD side, which is thus suggestive of conversion from MCI to AD. This is the premise underlying our approach.

The main contributions of our work are: 1) a novel image-based prognosticator of MCI-to-AD conversion that we will demonstrate to achieve both better generalization accuracy and much higher correlation with known brain region biomarkers than the CDR-based approach; 2) The finding that MCI subgroups that are strongly correlated with known AD brain region biomarkers are not so strongly correlated with “cognitive decline” as measured by MMSE; 3) Identification of the brain regions most critical for accurately discriminating between our “converter” and “nonconverter” groups, via application of margin-based feature selection (MFE) (Aksu et al., 2010) to brain image classification, and demonstration of MFE’s better performance than the well-known RFE method (Guyon et al., 2002) on this domain.

treat these individuals as outliers and omit them from our experiments.

2. Methods

2.1. Subjects and MRI data

We used T_1 -weighted ADNI images⁴ that have undergone image correction described at the ADNI website.⁵ ADNI aims to recruit and follow 800 research participants in the 55-90 age range: approximately 200 elderly Controls, 400 people with MCI, and 200 people with AD. The number of Control, MCI, and AD participants in our analysis were ≈ 180 , 300, and 120, respectively – experiment-specific detailed descriptions will be provided in Sec. 3. We processed the T_1 -weighted images as described in Appendix A, producing new images from which we then obtained the features (next discussed) used by our statistical classifiers.

2.2. Features for classification

We chose as features the voxel intensities of a processed⁶ RAVENS image, a type of “volumetric density” image (Davatzikos, 1998; Davatzikos et al., 2001; Goldszal et al., 1998; Shen et al., 2003) that has been validated for voxel-based analysis (Davatzikos et al., 2001) and applied both to AD e.g. (Davatzikos et al., 2010; Misra et al., 2009; Wang et al., 2010) and other studies e.g. (Fan et al., 2007)⁷. For each of the three processed RAVENS tissue maps (gray matter (GM), white matter (WM), and ventricle), to reduce

⁴ Data used in the preparation of this article were obtained from the Alzheimer’s Disease Neuroimaging Initiative (ADNI) database (adni.loni.ucla.edu). The ADNI was launched in 2003 by the National Institute on Aging (NIA), the National Institute of Biomedical Imaging and Bioengineering (NIBIB), the Food and Drug Administration (FDA), private pharmaceutical companies and non-profit organizations, as a \$60 million, 5-year public-private partnership. The primary goal of ADNI has been to test whether serial magnetic resonance imaging (MRI), positron emission tomography (PET), other biological markers, and clinical and neuropsychological assessment can be combined to measure the progression of mild cognitive impairment (MCI) and early Alzheimer’s disease (AD). Determination of sensitive and specific markers of very early AD progression is intended to aid researchers and clinicians to develop new treatments and monitor their effectiveness, as well as lessen the time and cost of clinical trials.

⁵ADNI image correction steps include Gradwarp, N3, and scaling for gradient drift – see www.loni.ucla.edu/ADNI/Data/ADNI_Data.shtml.

⁶We describe our processing of RAVENS images in Appendix A.

⁷Of particular interest, (Davatzikos et al., 2001) supported that voxel-based SPM statistical analysis, which we perform herein for comparison with our methods, can be performed on RAVENS images.

complexity for subsequent processing, we obtained a subsample by successively skipping five voxels along each of the three dimensions, and took as feature set the union of the three subsampled maps. We will also report results for the case of skipping only two voxels, rather than five.

Since high-dimensional nonlinear registration (warping) of all individuals to a common atlas (via HAMMER (Shen et al., 2002)) is applied in producing our features, they capture both volumetric and morphometric brain characteristics, which is important since individuals with AD/MCI typically exhibit brain atrophy (affecting both volume and shape).

2.3. Classification and feature selection for high-dimensional images

A challenge in building classifiers for medical images is the relative paucity of available training samples, compared to the huge dimensionality of the voxel space and, thus, to the number of parameters in the classifier model – in general, the number of parameters may grow at least linearly with dimensionality. In the case of 3D images, this could imply even millions of parameter values (e.g. one per voxel) need to be determined, based on a training set of only a few hundred patient examples. In such cases, classifier overfitting is likely, which can degrade generalization (test set) accuracy. Here we will apply a linear discriminant function (LDF) classifier with a built-in mechanism to avoid overfitting and with design complexity that scales well with increasing dimensionality - the support vector machine (SVM) (Vapnik, 1998). The choice of LDF achieving perfect separation (no classification errors) for a given two-class training set is not unique. The SVM, however, is the unique separating LDF that maximizes the *margin*, *i.e.* the minimum distance to the classifier decision boundary, over all training samples. In this sense, the SVM maximizes separation of the two classes. For an SVM, unlike a standard LDF, the number of model parameters is bounded by the number of training samples, rather than being controlled by the feature dimensionality. Since the number of samples is the much smaller number for medical image domains, in this way the SVM greatly mitigates overfitting. SVMs have achieved excellent classification accuracy for numerous scientific and engineering domains, including medical image analysis, (Aksu et al., 2010; Davatzikos et al., 2010; Guyon et al., 2002).

Even though SVMs are effective at mitigating overfitting, generalization accuracy may still be improved in some cases by removing features that contribute little discrimination power. Moreover, even if generalization accuracy monotonically improves with increasing feature dimensionality, high

complexity (both computation and memory storage) of both classifier design and class decisionmaking may outweigh small gains in accuracy achieved by using a huge number of features. Most importantly here, it is often useful to identify the critical subset of features necessary for achieving accurate classification – these “markers” may shed light on the underlying disease mechanism. In our case, this will help to identify prognostic brain regions, associated with MCI conversion.

Unfortunately, there is a huge number of possible feature subsets, with exhaustive subset evaluation practically prohibited even for modest number of features, M , let alone $M \sim 10^6$. Practical feature selection techniques are thus heuristic, with a large range of tradeoffs between accuracy and complexity (Guyon et al., 2003). “Front-end” (or “filtering”) methods select features prior to classifier training, based on evaluation of discrimination power for individual features or small feature groups. “Wrapper” methods are generally more reliable, interspersing sequential feature selection and classifier design steps, with features sequentially selected to maximize the current subset’s joint discrimination power. There are also embedded feature selection methods, e.g. for SVMs, use of ℓ_1 -regularization within the SVM design optimization (Fung et al., 2004), in order to find “sparse” weight vector solutions, which effectively eliminate many features. For wrappers, there is greedy forward selection, with “informative” features added, backward elimination, which starts from the full set and removes features, and more complex bidirectional searches. In our work, due to the high feature dimension, we focus on two backward elimination wrappers that afford practical complexity: i) the widely used recursive feature elimination algorithm (RFE) (Guyon et al., 2002), where at each step one removes the feature with least weight magnitude in the SVM solution. RFE has been applied before to AD (Davatzikos et al., 2010; Misra et al., 2009; Wang et al., 2010); ii) the recent margin-based feature elimination (MFE) algorithm (Aksu et al., 2010), which uses the same objective function (margin) for feature elimination, one consistent with good generalization, that the SVM uses for classifier training (Vapnik, 1998). MFE was shown in (Aksu et al., 2010) to outperform RFE (Guyon et al., 2002) and to achieve results comparable to embedded feature selection for domains with up to 8,000 features (gene microarray classification). Here we will also find that MFE gives better results than RFE.

2.4. An MRI-Derived Alternative to CDR-based MCI-to-AD Conversion

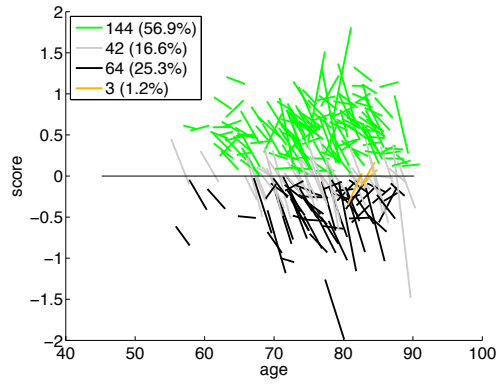
In the Introduction, we outlined our two classifier design steps for building an automatic prognosticator for an individual with MCI. In this section, we elaborate on these two steps and give an illustrative example. Our AD-Control classifier, used in the first step, is discussed in Sec. 2.4.1, and our second classifier, used to discriminate converter-by-trajectory (CT) and nonconverter-by-trajectory (NT) classes, is discussed in Sec. 2.4.2.

2.4.1. AD-Control classifier

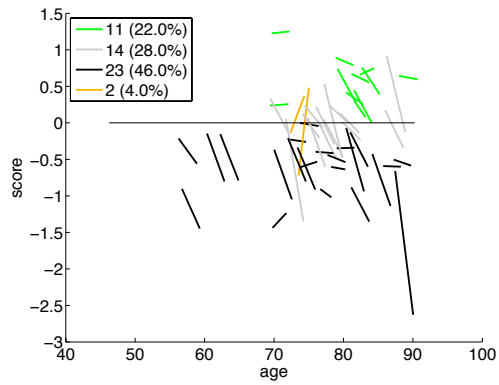
For the AD training population, we chose individual AD visit images with a CDR score of at least 1. For the Control training population, on the other hand, we only chose *initial* visits, and only those for participants who stayed at CDR=0 throughout all their visits. Thus, we excluded Controls with “questionable dementia” (i.e., CDR=0.5) at any visit. By these choices, we sought to exclude outlier examples or even possibly any mislabeled examples, recalling that CDR for the majority of both AD and MCI participants is 0.5 throughout all visits.

2.4.2. CT-NT classifier

Fig. 1 gives an illustrative example of the phenotypical score trajectories for MCI subject described in the Introduction. A positive score is on the Control side and a negative score is on the AD side – the x-axis represents the AD-Control SVM’s decision boundary. Score vs. age is plotted, with each line segment a trajectory obtained by linearly fitting an individual’s phenotype scores (and linearly extrapolating if there are missing visits). Nonconverters-by-CDR (N-CDR) and converters-by-CDR (C-CDR) are illustrated in (a) and (b), respectively. Green and black subjects are those whose fitted trajectory stayed on the Control side and AD side, respectively, whereas gray lines are subjects who crossed to the AD side. Thus, by our conversion-by-trajectory definition, the green group is the nonconverters-by-trajectory, and the black and gray groups together are the converters-by-trajectory. Subject counts for these groups are given in the figure legends. The outlier subjects are shown in orange – there are five, making up less than 2% of the MCI cohort. Notice, intriguingly, from the left figure that more than one third of all (non-orange) MCI patients (106 of 298) are converters by trajectory and yet nonconverters according to CDR – *i.e.*, there is a very large percentage of patients for which the two converter definitions disagree, with the neuroimage-based definition indicating disease state changes that are not



(a)



(b)

Figure 1: AD-Control SVM score trajectories for MCI subjects. (a) Nonconverters-by-CDR. (b) Converters-by-CDR.

predicted using the clinical, CDR-based definition. Likewise, an additional 3% of all MCI subjects (11 of 298) “defy” their by-CDR converter label in that they do not reach the AD side of the decision boundary.

Based on these trajectories, i.e. whether or not the AD side is visited, we derive the ground-truth ‘CT’ and ‘NT’ labels for all MCI subjects. We then build a CT-NT classifier using as input *only* the image scans at initial visit.⁸

3. Results and Discussion

3.1. Introductory overview

In this section we will perform 1) classification experiments to evaluate conversion-by-trajectory and conversion-by-CDR with respect to desideratum 2; 2) additional experiments to compare the two definitions with respect to desideratum 3; and lastly, 3) experiments to identify prognostic brain “biomarker” regions.

It is important to mitigate the potential confounding effect of the subject’s age. In our classification experiments, we mitigated in two ways:

1) For every classifier training, each training sample in one class was uniquely paired via “age-matching” with a training sample in the other class (with age separation at most one year).

2) For every linear-kernel SVM classifier, we separately adjusted each feature for age prior to classification using linear fitting. We subtracted the extrapolated line (computed only using “control” samples⁹) from the feature’s value, for all (training and test) samples. As an aside, we note that, given the subsequent linear SVM operation, the representation power of this linear fitting step is essentially equivalent to simply treating age as an additional feature input to the linear SVM classifier.

Finally, prior to building classifiers, we normalized feature values to the [0,1] range, which is suitable for the LIBSVM software (Chang et al., 2001) we used for training SVMs.

⁸For a small percentage of the MCI subjects, we did not obtain the patient’s first visit. However, we did ensure that the visit we took as the “initial visit” had a CDR of 0.5.

⁹For the AD-Control classifier, these are the samples in the Control class. For the CT-NT classifier we computed the line using only the NT samples.

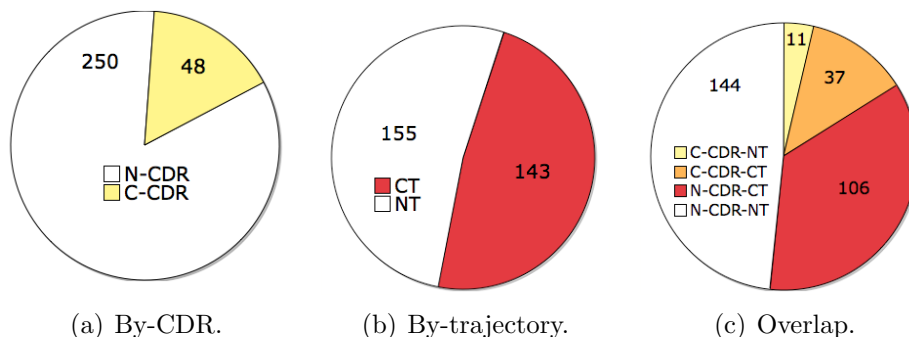


Figure 2: A population of 298 MCI subjects in ADNI is shown here, broken up according to the two criteria discussed in Sec. 3.2.1: (a) by-CDR criterion, (b) by-trajectory criterion; with overlap shown in (c).

3.2. Experiments with voxel-based features

The test set (generalization) accuracy of the voxel-based AD-Control classifier, built using 70 training samples per class, was 0.89 (86 of 88 Controls, and 16 of 27 AD subjects, were correctly classified.) This classifier, with high specificity for Controls, was then applied to a population of MCI subjects to determine the CT and NT subgroups.

3.2.1. Classification experiments for the MCI population

Fig. 2(a) shows the sizes of the converter-by-CDR (C-CDR) and nonconverter-by-CDR (N-CDR) groups within the ADNI MCI cohort for a typical experiment in our work. Fig. 2(b) shows the same population broken up as converters-by-trajectory (CT) and nonconverters-by-trajectory (NT). Superimposing the two charts, Fig. 2(c) illustrates their overlap, where converters by both definitions are accordingly indicated by orange. Since converters-by-CDR are relatively scarce, we used a large majority of them (80%, i.e. 39 individuals among the 48) for the by-CDR classifier’s training set, with the rest (20%) put into the test set. We reiterate that a general disadvantage of the by-CDR approach is its scarcity of converter examples – by contrast, a more balanced number of examples is available for by-trajectory training (at least 100, rather than 39, training samples per class, as in Fig. 2(b)). Note also that if we were to use a “probable AD”, rather than a by-CDR converter definition, there would be even *fewer* converter examples.

A fair performance comparison between by-trajectory and by-CDR classification requires: 1) using the same per-class training set size (i.e. 39) for

both by-CDR and by-trajectory training, *and* 2) making the test set sizes the same for both classifiers. There are several different ways in which the data can be partitioned into training and test sets, consistent with these two conditions: i) we can perform simple random selection on a class-by-class basis, ensuring only that the two classifiers are given the same training/test set *sizes* (but not the same *sets*);¹⁰ ii) we can make the training sets of the two classifiers *identical* rather than *merely same-sized*, as well as make the test sets identical. This latter approach, though, will have some bias because, in selecting samples for the by-trajectory classifier, we will have to make use of knowledge of the samples’ conversion-by-CDR status (and vice versa for the by-CDR classifier). The first approach, on the other hand, clearly does not have this bias. As both approaches are valid ways of dealing with by-CDR data limitations, we will compare generalization accuracies of by-CDR and by-trajectory classifiers under both these data selection schemes, referring to these approaches as “random” and “identical” in the sequel.

Our training/test set selection procedure for the “identical approach” is as follows. For the C-CDR-CT group (Fig. 2(c)), randomly select 80% of the group (the yellow striped group of size 30 in Fig. 3(a)) such that a corresponding group within N-CDR (white portion in Fig. 2(a)) can be found that is both *NT* and satisfies age-matching. This corresponding group is illustrated in Fig. 3(a) as the white striped group (of size 30), placed opposite from the yellow striped area it is paired (matched) with. Likewise for the C-CDR-NT group (Fig. 2(c)), randomly select 80% of the group (the yellow striped group of size 9 in Fig. 3(a)) such that a corresponding group within N-CDR can be found that is both *CT* and satisfies age-matching. This corresponding group is illustrated in Fig. 3(a) as the white striped group (of size 9). Notice by comparing this figure to Fig. 2(c) that the two white striped areas are separated by the CT-NT border. We take the training set – shared by the by-CDR and by-trajectory classifiers – to be precisely the union of these four striped areas.¹¹ Subsequently, we take the test set –

¹⁰Note that this means that the training sets for the converter and nonconverter classes of the conversion-by-CDR classifier are randomly selected from the yellow and white regions in Fig. 2(a), respectively, with *no* consideration of trajectory-based (i.e. red/white) labeling illustrated in Fig. 2(b).

¹¹For the by-CDR classifier, the class membership of any of these four subsets of the training set is illustrated by the color being yellow or white in Fig. 3(a). Likewise, for the by-trajectory classifier, class membership is illustrated by red or white color in Fig. 3(b).

shared by the two classifiers – to be the subjects who are neither in 1) the training set (striped areas) nor in 2) the special set of subjects shown in solid gray in Fig. 3(a) (also shown identically in Fig. 3(b)).¹² That is, the test set is the tiled areas in Fig. 3(a) (or, identically, in Fig. 3(b)).

Note above that *some* random selection is being employed in choosing the training/test sets even in the “identical approach” (whereas, in the “random approach” the selection is completely random). Thus, for both approaches, the accuracy of performance comparison will benefit from averaging accuracy results over multiple training/test split “trials”. Results averaged across 10 trials are given in Fig. 3(c) for a linear-kernel SVM¹³; $\mu \pm \sigma$ notation is used to indicate the mean μ and standard deviation σ of quantities across the trials.¹⁴ Note that by-trajectory’s generalization performance is as high as 0.83, whereas by-CDR’s generalization performance is very poor – *as poor as random guessing* (see 0.5 and 0.56 table values) – due mainly to poor performance on *nonconverters*-by-CDR. Fig. 3(d) and Fig. 3(e) show by-trajectory and by-CDR results, respectively, for one of the 10 trials (for the “random approach”), with each bar indicating distance to the classification boundary¹⁵ for an MCI subject in a test population of size 88 and non-converters/converters shown in left/right figures, respectively. Among the 88 subjects, by-trajectory correctly classified 79 whereas by-CDR correctly classified only 40.

Recently, similarly poor by-CDR classification performance was also reported in (Davatzikos et al., 2010), where it was found that the majority of (by-CDR) nonconverters “had sharply positive SPARE-AD scores indicating significant atrophy similar to AD patients”. Since the SPARE-AD score is produced by a classifier that was trained to discriminate Control and AD patients (Fan et al., 2007, 2008), this comment and associated results are consistent both with our conjecture in the Introduction and our above

¹²We exclude this “special set” (in gray) from the *test set* so that *all* our experiments under the “identical approach” can have a shared, fixed test set (for fair comparison with each other), including, crucially, an experiment that will include this “special set” of samples in the *training set*.

¹³For generating all classification results herein, including those in Fig. 3(c), we used SVM classifiers that were built by employing the common approach of bootstrap-based validation for selecting the classifier’s (trial’s) hyperparameter values (Aksu et al., 2010).

¹⁴ μ and σ of integer quantities (e.g. sample counts) are shown rounded up.

¹⁵Positive/negative distance means nonconverter/converter side of the boundary, respectively.

histogram results, which suggest that there may be a significant number of patients undergoing physiological brain changes consistent with conversion, yet without clinical manifestation.

The results above indicate that the conversion-by-CDR definition’s two classes are not well-discriminated, and thus, clinical usefulness of this definition for our prognostic Aim is expected to be poor. The much greater generalization accuracy of the by-trajectory definition (coupled with its inherent plausibility as a conversion definition) indicates its greater utility.

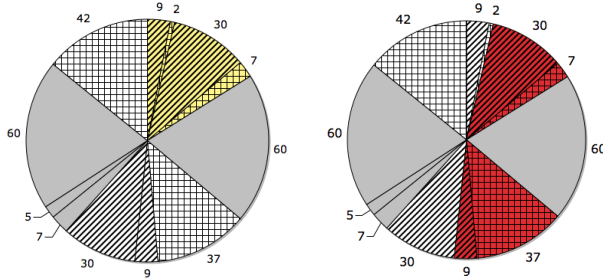
Increasing the By-Trajectory Image-Based Feature Resolution:

In a separate experiment, we evaluated using one of 27 subsamples (rather than one of 216 subsamples), i.e. essentially a 10-fold increase in the number of (voxel-based) features, and found that the by-trajectory generalization accuracy rose to 0.91 in the “random” case. We then tried building 27 separate by-converter classifiers, one for *every* 1/27th subsample (thus effectively using the whole 3D image), with majority-based voting used to combine the 27 decisions. This ensemble scheme again achieved 0.91 accuracy, i.e. there was no further accuracy benefit beyond that from an \approx 10-fold increase in the number of voxel features.

Increasing the By-Trajectory Training Set Size

Note that the converter-by-CDR sample scarcity and class-balancing (via age-matching) in the experiments above had the effect of artificially limiting the *by-trajectory* classifier training set size. Next we investigated how much the generalization accuracy of by-trajectory classification improves when this limitation is removed. The tiled areas in Figures 4(a) and 3(b) are identical, illustrating that in this new experiment (Fig. 4(a)) we used the same test set as previously, for fairness of comparison. However, as indicated by differences in the total striped area between these two charts, we now make the training set much larger than previously. Specifically, for the “identical” case, we used the previous 10 trials but simply augmented a trial’s training set with the two large, previously-excluded gray sets¹⁶, as these two sets do age-match each other. The results, averaged across the 10 trials, are given in Fig. 4(b). Notice in this figure the now larger per-class training size (on average \approx 100 rather than 39), and that the random approach uses this size as well. The by-trajectory results in Fig. 4(b) indicate that accuracy improved from 0.78 ± 0.02 (Fig. 3(c)) to 0.84 ± 0.02 for the “identical approach”,

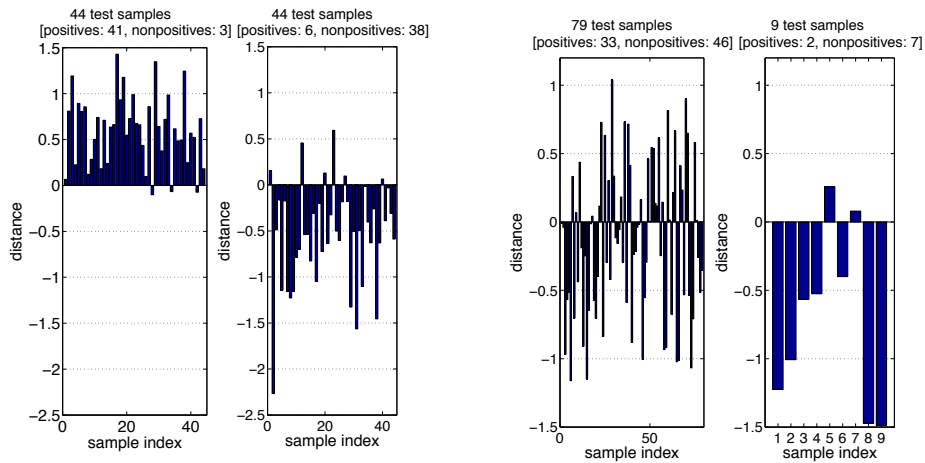
¹⁶Shown in Fig. 3(b), with size 60. Note that this size can vary from trial to trial.



(a) Training/test set selection for by-CDR classification. (b) Training/test set selection for by-trajectory classification.

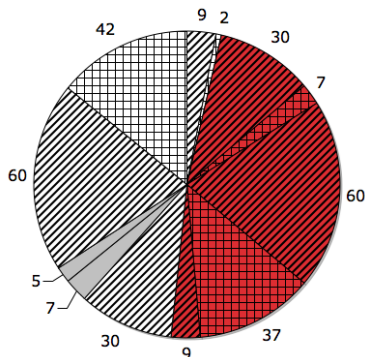
Sample selection	Classifier	Test set				Overall accuracy
		Converters		Nonconverters		
		Count	Accuracy	Count	Accuracy	
Random approach	By-trajectory	46 ± 1	0.81 ± 0.06	45 ± 1	0.84 ± 0.05	0.83 ± 0.05
	By-CDR	9 ± 1	0.79 ± 0.07	82 ± 2	0.47 ± 0.04	0.50 ± 0.04
Identical approach	By-trajectory	45 ± 1	0.78 ± 0.04	47 ± 2	0.78 ± 0.04	0.78 ± 0.02
	By-CDR	9 ± 1	0.74 ± 0.11	82 ± 2	0.54 ± 0.04	0.56 ± 0.04

(c) Average test set classification accuracy using all 11, 293 features, 39 ± 1 per-class training samples.



(d) By-trajectory. Left: nonconverters; Right: converters (e) By-CDR. Left: nonconverters; Right: converters

Figure 3: Test set accuracy comparison of by-CDR and by-trajectory classification.



(a) Training/test set selection for by-trajectory classification.

	Sample selection	Test set				Overall accuracy
		Converters		Nonconverters		
		Count	Accuracy	Count	Accuracy	
By-trajectory	Random	45 ± 1	0.77 ± 0.01	47 ± 2	0.86 ± 0.02	0.82 ± 0.01
	Identical	45 ± 1	0.85 ± 0.03	47 ± 2	0.83 ± 0.05	0.84 ± 0.02

(b)

Figure 4: By-trajectory average test set classification accuracy for the larger training set size (98 ± 1 per class) and 11,293 features.

and modestly worsened for the “random approach” (from 0.83 ± 0.05 to 0.82 ± 0.01).

Evaluating a Third Conversion Definition

We now consider a third definition of conversion that combines the first two definitions as follows. Let “converters” consist of individuals who converted either by-trajectory *or* by-CDR (non-white areas in Fig. 2(c)), with the “nonconverter” class consisting of the remaining MCI individuals (white area). The point of view of this new definition, “conversion-by-union”, is to be more inclusive in defining an MCI subpopulation at risk, which may benefit from early treatment or diagnostic testing. While from that perspective the new definition is reasonable, the fact that grouping individuals by CDR has a role in this definition may be its disadvantage, considering that by-CDR classification was previously shown to perform not much better than random guessing. Results, averaged across the same 10 trials used in Fig. 3, are given in Table 1 and indicate that conversion-by-union generalizes somewhat

	Sample selection	Test set				Overall accuracy
		Converters		Nonconverters		
		Count	Accuracy	Count	Accuracy	
By-union	Identical	48 ± 1	0.78 ± 0.05	44 ± 2	0.75 ± 0.06	0.77 ± 0.03

Table 1: Average test set accuracy of by-union classification for 39 ± 1 per-class training samples and 11,293 features.

worse than conversion-by-trajectory.¹⁷

3.2.2. Validation on Known AD Conversion Biomarkers

To validate the proposed conversion definitions with respect to desideratum 3, we performed correlation tests on the MCI population between the binary class variable $C \in \{0 = \text{no conversion}, 1 = \text{conversion}\}$ and known AD conversion biomarkers consisting of both 1) volume in reported AD-affected regions (Table 2 in (Schuff et al., 2010)), which we measured for each individual’s *final-visit* MRI¹⁸ and 2) the clinical MMSE measure. The stronger the correlation, the more accurately the biomarker is predicted from the class variable and the greater the separation between the biomarker histograms, conditioned on the two classes.

Before presenting correlation test results, we first illustrate in Fig. 5 the increased separation of the histograms of hippocampus volume for the converter and nonconverter groups in the by-trajectory case, compared with by-CDR. Next, we performed comprehensive statistical tests for a number of suggested AD biomarkers. The R statistical computing package was used to perform all tests with statistical significance set at the 0.05 level. In Table 2a

¹⁷Note that “by-union” is, by definition, an instance of the “identical approach”, as stated in Table 1. To ensure fairness of comparison with the by-trajectory definition of conversion, our test sets, and training set sizes, in these two cases were identical. In fact, we chose the by-union training set to be as similar to by-trajectory’s, in every trial, as possible. Referring to Fig. 3(b) (which represents a trial example), the by-union training set was chosen to include 1) the two large striped groups (red and white); 2) the small “special” gray group (of size seven in this trial example) and its age-matched counterpart within small white-striped group, and; 3) a subset of the second small “special” gray group (two of five individuals in this trial example) and its age-matched counterpart within the small red-striped group.

¹⁸As discussed in Appendix A, we measured *normalized* region volume. Note also that our regions are defined based on the atlas (Atlas2) we used. The correspondence between the regions in (Schuff et al., 2010) and our defined regions is given in Appendix B. Finally, note that a subject’s final visit is not always the sixth visit.

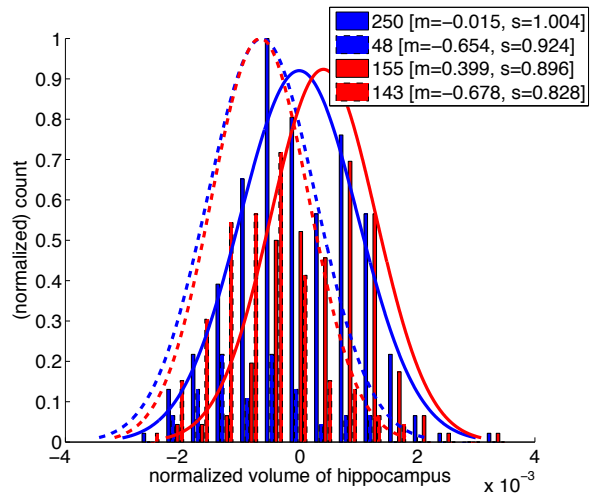


Figure 5: For the hippocampus, by-trajectory (red) has larger histogram separation between converter (dashed line) and nonconverter (solid line) groups than by-CDR (blue). To illustrate this more clearly, also shown is the Gaussian curve for each of these four subject groups (plotted based on group mean (m) and standard deviation (s) indicated in the figure legend with the same 0.001 scaling as the x-axis).

(and Fig. 6), the correlation coefficients for by-trajectory and by-CDR are shown for each biomarker, along with their associated p-values (Chambers et al., 1993). Note that for 11 out of 14 brain regions, the correlation with by-trajectory is greater than the correlation with by-CDR (in **bold**), with by-trajectory meeting the significance threshold in 10 of these 11 regions. Further, for only two of the remaining four biomarkers - posterior cingulate and the clinical MMSE measure - does the correlation with by-CDR meet the significance threshold. Most notably, well-established markers for AD such as the hippocampus, lateral ventricles, and inferior parietal exhibited strong correlation with the by-trajectory definition.

To further assess statistical significance of the *comparison* between by-trajectory and by-CDR correlations, we performed a correlated correlation test (Meng et al., 1992), the appropriate test given that the same MCI sample population was used in measuring correlations for both by-CDR and by-trajectory. This test (Table 2b) reveals that the larger correlation of by-trajectory is statistically significant at the 0.05 level in nine brain regions (in **bold**). By contrast, conversion-by-CDR does not achieve a statistically significant advantage for any of the brain regions, nor with respect to MMSE. To mitigate the confounding effect of age in the AD biomarker measurements, we linearly adjusted them for age prior to performing the experiments described above. We also repeated these experiments without age adjustment. In this case, the number of regions for which by-trajectory’s correlation exceeded by-CDR’s rose from 11 to 12 (with the addition of the entorhinal cortex), and the number of regions for which the larger correlation of by-trajectory was statistically significant rose from 9 to 10 (with the addition of the medial orbitofrontal GM).

3.2.3. Identification of prognostic brain “biomarker” regions

In the previous section, we validated conversion definitions using established (diagnostic) AD biomarker brain regions (with volumes measured at final visit). In this section, we will *identify* key *prognostic* biomarker brain regions via supervised feature selection, aiming first to identify the “essential” subset of voxel features, i.e. the voxels (at initial visit) necessary for our classifier to well-discriminate the CT and NT classes. The brain regions (consistent with a registered brain atlas) within which these select voxels principally reside then identify our prognostic brain biomarker regions. Similarly, we will identify *diagnostic* regions, critical for discriminating between AD and Control subjects (using our AD-Control classifier). In both cases,

(a)

Biomarker	By-trajectory		By-CDR	
	Correlation coefficient	P-value	Correlation coefficient	P-value
Entorhinal cortex	0.041	0.486	0.050	0.385
Fusiform gyrus	0.430	8.20E-15	0.152	0.008
Hippocampus	0.530	2.00E-16	0.231	5.67E-05
Inferior parietal GM	0.513	2.00E-16	0.097	0.094
Lateral orbitofrontal GM	0.077	0.185	0.078	0.178
Lateral ventricles	0.586	2.00E-16	0.211	0.000246
Medial orbitofrontal GM	0.239	3.01E-05	0.101	0.081
Parahippocampal gyrus	0.095	0.102	0.060	0.307
Posterior cingulate	0.001	0.981	0.144	0.013
Precentral GM	0.173	0.003	0.088	0.128
Superior frontal GM	0.331	4.50E-09	0.094	0.104
Superior temporal GM	0.478	2.00E-16	0.161	0.005
Total GM	0.491	2.00E-16	0.246	1.70E-05
Total WM	0.170	0.003	0.041	0.477
MMSE	0.356	2.57E-10	0.453	2.00E-16

(b)

P-value
0.889
2.17E-06
2.42E-10
0.985
1.34E-09
0.048
0.616
0.045
0.230
0.001
3.10E-05
0.0001
0.069
1.33E-06
0.118

Table 2: Correlation coefficients and associated p-values: (a) Correlation test results; (b) Correlated correlation test results for each of the regions in (a). Statistically significant results are shown in bold.

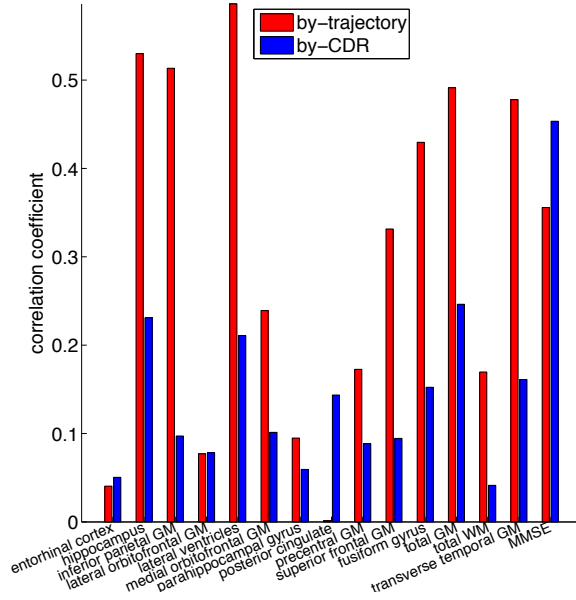


Figure 6: Comparison of correlation coefficients for by-trajectory and by-CDR.

AD-Control classifier only	intersection	CT-NT classifier only
Amygdala left	Hippocampal formation* left	Superior temporal gyrus* left
Cingulate region right	Hippocampal formation* right	Middle temporal gyrus left
Entorhinal cortex right	Entorhinal cortex* left	Precuneus right
Inferior occipital gyrus right	Inferior temporal gyrus right	Lateral front-orbital gyrus* right
Medial occipitotemporal gyrus left	Lateral occipitotemporal gyrus* right	Insula right
Parahippocampal gyrus left	Parahippocampal gyrus* right	Supramarginal gyrus* left
Temporal lobe WM right	Perirhinal cortex left	Temporal lobe WM left
Temporal pole right	Perirhinal cortex right	Temporal pole left
	Middle temporal gyrus right	Medial front-orbital gyrus* left
	Uncus left	

Table 3: Brain regions identified as biomarkers using voxel-based features and MFE.

the accuracy of the selected brain region biomarkers rests heavily on the accuracy of the supervised feature selection algorithm we employ. In Figures 7(a) and 7(b), we compare MFE and RFE feature elimination (i.e. feature selection via feature elimination) for both Control-AD classification and for CT-NT classification (for one representative, example trial). The curves show test set accuracy as a function of the number of retained features (which is reduced going from right to left). Note that the “MFE/MFE-slack” hybrid method (Aksu et al., 2010)) outperforms RFE for both brain classification tasks, achieving lower test set error rates, and with much fewer retained features. The circle, determined without use of the test set based on the rule in (Aksu et al., 2010), marks the point at which we stopped eliminating features by MFE, thus determining the (trial’s) retained voxel set. This MFE-RFE comparison (and the previous comparison in (Aksu et al., 2010)) supports our use of MFE to determine brain biomarkers.

To relate the retained voxel set to anatomic regions in the brain, we overlaid the retained voxel set onto a registered atlas space. For CT-NT classification, to improve robustness, the final voxel set was formed from the union of the retained voxel sets from each of ten feature elimination trials (each using a different, randomly selected training sample subset). For AD-Control classification, the final voxel set came from a single trial (the only trial, from which the 10 CT-NT trials stemmed). For each of these two cases, overlaying the final voxel set onto the co-registered atlas (Atlas2, defined in Appendix A) yielded between 70-80 anatomic regions. For data interpretation purposes, we then identified a subset of (biomarker) regions using the following procedure. First, for each brain region, we measured the percentage of the region’s voxels that are retained, *sorted* these percentages, and then plotted them. As shown in Fig. 8(a), the resulting curve for the AD-Control case has a distinct knee, which we thus used as a threshold (0.125) to select the final, retained (diagnostic) regions for AD-Control. We used the same threshold for the CT-NT curve, shown in Fig. 8(b). This choice of threshold yields a reasonable number of regions – 19 for the CT-NT (prognostic) case and 21 for the AD-Control (diagnostic) case.

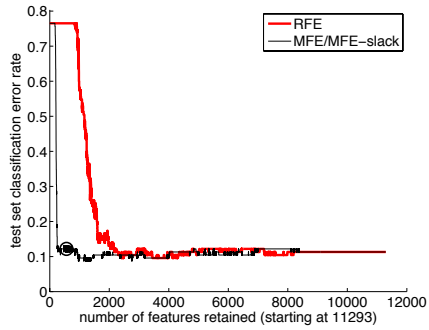
The resulting sets of identified prognostic and diagnostic biomarkers are given in Table 3, along with their intersection. The diagnostic markers in the table include the majority of the known brain regions in the medial temporal lobe involved in AD pathology. For example, hippocampus atrophy and lateral ventricle enlargement, particularly in its anterior aspects of the temporal horn, are considered the most prominent diagnostic markers for AD.

Entorhinal cortical regions, including the perirhinal cortex, are presumably the earliest sites of degeneration (Braak et al., 1997). Thus, independent identification by our AD-control classifier of known AD diagnostic biomarkers establishes a reasonable basis for applying the same approach to identify prognostic biomarkers. The brain regions listed as CT-NT prognostic markers include most known AD diagnostic markers (including 8 of the 12 regions from (Schuff et al., 2010) (marked by *), 4 of which are also diagnostic markers), indicating that some AD-linked pathological changes in these brain regions already occurred and remained active in a subset of MCI subjects who likely progress to AD rapidly. Conversely, the brain areas appearing only on the prognostic marker list are likely the most active areas of degeneration during this stage of progression to dementia. These structures tend to be the brain regions further away from the entorhinal cortex onto the parietal (Supramarginal gyrus, Precuneus) and temporal cortex (Superior temporal gyrus and Middle temporal gyrus) regions. All the brain structures listed in the table are known to be involved in AD (Braak et al., 1997; Chan et al., 2003; Frisoni et al., 2009). Thus, the markers in Table 3 suggest an interesting anatomic pattern of trajectory for MCI conversion to AD which conforms with the Braak and Braak hypothesis and previous imaging findings (Chan et al., 2003; Frisoni et al., 2009). Moreover, the CT-NT regions uniquely found by our MFE-based procedure in Table 3 may be viewed as “putative” prognostic markers, and may warrant further investigation.

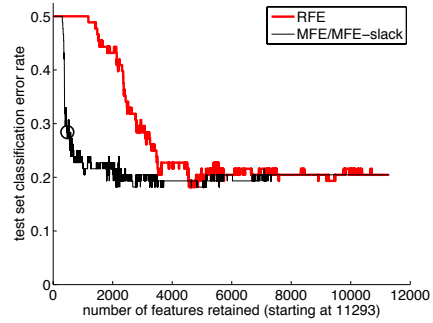
Finally, we note that we have used a particular criterion (percentage of a region’s voxels that are retained) to identify biomarker regions, starting from MFE-retained voxels. While our identified regions are plausible, it is possible that other (equally reasonable) criteria may produce different biomarker region results. Thus, the biomarkers we identify should be viewed as anecdotal, identifying regions that figure prominently in our classifier’s decisionmaking and also potentially assisting researchers in forming hypotheses about MCI-to-AD disease progression. However, we do not view the identified regions as definitive.

3.2.4. Comparison with an SPM-based biomarker identification approach

In the previous section, we used MFE to identify voxels as biomarkers for the CT and NT classes. Here, using the same CT-NT training and test populations, we will alternatively identify voxel-based biomarkers using statistical testing with SPM5 (see: (SPM website)). Subsequently we will present a classifier generalization accuracy comparison (where accuracy

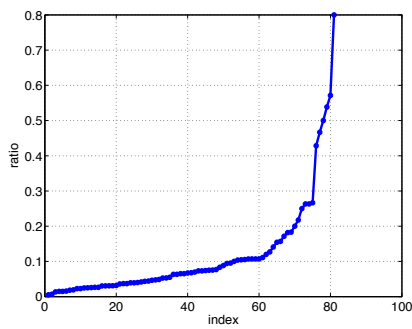


(a)

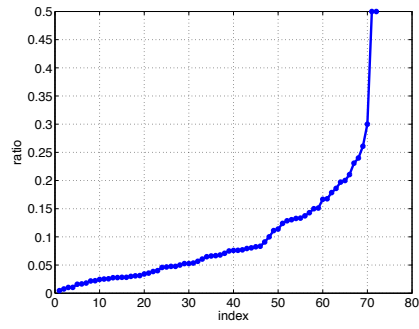


(b)

Figure 7: Test set misclassification rate during the course of feature elimination, for (a) the AD-Control classifier and (b) the CT-NT classifier.



(a)



(b)

Figure 8: Sorted retained voxel percentages for initial regions (a) AD-Control; b) CT-NT, used to select final regions (Sec. 3.2.3).

is again measured on the previous section’s CT-NT (*test*) population) for these two biomarker detection methods. We determined SPM biomarkers as follows. The CT-NT training set population, being age-matched, is readily suitable for a paired t-test, an appropriate statistical test for determining SPM-identified biomarkers, i.e. voxels that discriminate between the CT and NT groups. In contrast with MFE’s use of *only one* (out of 216) RAVENS subsamples (taken jointly from the GM, WM, ventricle maps), we performed t-tests on *whole* RAVENS maps (without subsampling), which makes the SPM-MFE comparison favorably biased towards SPM. More specifically our steps were as follows. First, for the GM and WM maps separately, we found using SPM that a large portion of each of these two tissues was statistically significant at the 0.05 level when correction for multiple comparisons was not applied. Next, we used SPM’s FDR-based correction for multiple comparisons – based on an SPM FDR cluster size of 5 voxels we found that the spatial extent of the statistically significant regions, at each of the levels 0.05, 0.01, and 0.005, was approximately a subset of the above-mentioned spatial support found in the uncorrected case. Given that the number of significant voxels in any of these SPM experiments is, again due to no subsampling, much larger than the 11,293 voxels started from in the MFE case, we simply 1) chose as our SPM result the result for 0.01 (FDR-corrected), 2) took from among those significant voxels the *most* significant 11,434 voxels in order to be able to compare MFE and SPM for \approx the same number of voxels (biomarkers). To obtain the generalization accuracy for this SPM-identified biomarker voxel set, using the same training/test set as in the MFE experiment, we trained an SVM classifier and measured its generalization accuracy, which was found to be 0.76. This accuracy is somewhat lower than the 0.8 accuracy of the previous section’s CT-NT SVM classifier. Recalling that this comparison is actually favorably biased towards SPM, and further noticing the fact that MFE was able to maintain the 0.8 accuracy all the way down to 2000 features (cf. Fig. 7(b)), this experimental comparison provides another validation (beyond the comparison with RFE given earlier) for MFE-based feature/biomarker selection, applied to brain images.

4. Conclusions

We have presented an automated prognosticator of MCI-to-AD conversion based on brain morphometry derived from high resolution ADNI MR images. The primary novel contributions of our work are: i) casting MCI

prognostication as a novel machine learning problem lying somewhere between supervised and unsupervised learning; ii) our proposal of a conversion definition which, unlike previous methods, exploits both rich phenotypical information in neuroimages and AD and control examples; iii) correlation testing and classifier accuracy evaluations to validate candidate conversion definitions; iv) prognostic biomarker discovery based on our conversion definition. We demonstrated that our method achieved both better generalization accuracy and stronger, statistically significant, correlations with known brain region biomarkers than a predictor based on the clinical CDR score, the approach used in several past works. The brain structures identified as AD-control diagnostic markers and MCI conversion prognostic markers well conform with known brain atrophic patterns and progression trajectories occurring in AD-afflicted brains. While the noisy nature of cognitive assessments, including MMSE, has been acknowledged in past works, in future we may extend our methodology to consider cognitive assessment data, both potentially as additional (baseline) input features and as additional or alternative prediction targets to our “conversion-by-trajectory” labels. We may also consider alternative ways to adjust for confounding effects of age, noting that (Schuff et al., 2010) has characterized the nonlinear dependence of age on brain region volumes. Finally, while we have focused on the MCI subpopulation here, our system could also potentially be used to detect, as possible misdiagnoses, subjects diagnosed as “Control” who are classified as MCI converters by our system.

5. Acknowledgement

Funding supporting this work has been provided in part through NIH R01 AG02771 and the Pennsylvania Department of Health. We thank Dr. Michelle Shaffer for assistance with statistical testing and Jianli Wang and Zachary Herse for assistance with segmentation.

Data collection and sharing for this project was funded by the Alzheimer’s Disease Neuroimaging Initiative (ADNI) (National Institutes of Health Grant U01 AG024904). ADNI is funded by the National Institute on Aging, the National Institute of Biomedical Imaging and Bioengineering, and through generous contributions from the following: Abbott, AstraZeneca AB, Bayer Schering Pharma AG, Bristol-Myers Squibb, Eisai Global Clinical Development, Elan Corporation, Genentech, GE Healthcare, GlaxoSmithKline, Innogenetics, Johnson and Johnson, Eli Lilly and Co., Medpace, Inc., Merck

and Co., Inc., Novartis AG, Pfizer Inc, F. Hoffman-La Roche, Schering-Plough, Synarc, Inc., as well as non-profit partners the Alzheimer’s Association and Alzheimer’s Drug Discovery Foundation, with participation from the U.S. Food and Drug Administration. Private sector contributions to ADNI are facilitated by the Foundation for the National Institutes of Health (www.fnih.org). The grantee organization is the Northern California Institute for Research and Education, and the study is coordinated by the Alzheimer’s Disease Cooperative Study at the University of California, San Diego. ADNI data are disseminated by the Laboratory for Neuro Imaging at the University of California, Los Angeles. This research was also supported by NIH grants P30 AG010129, K01 AG030514, and the Dana Foundation.

Appendix A. Image processing

The input to our processing is a T_1 -weighted MR image of the head. First, using rigid-body registration implemented in FSL’s linear image registration tool FLIRT (Jenkinson et al., 2001), we coarsely aligned this (3d) image with the MNI/ICBM atlas resampled to 1mm isotropic voxel dimensions (aka Atlas1). We used FSL version 3 (see: (FSL website)). Next, we removed non-brain anatomy from the aligned head image, using FSL’s brain extraction tool BET (Smith et al., 2002). We then segmented the resulting brain-only 3d image into the following five segments required by HAMMER(Shen et al., 2002)¹⁹ : WM, GM, ventricles, (non-ventricle) CSF, (non-anatomy) background. Next, using as inputs an MNI atlas distributed with HAMMER (aka Atlas2²⁰) and the ADNI participant’s five-segment image, we performed two different HAMMER operations, generating: 1) the three “volumetric density” Ravens images: GM, WM, ventricles. The union of these three images (following some preprocessing) forms the set of features used by our classifier; 2) the 3d region-segmented image, whose region volumes are used for by-trajectory statistical validation in section 3.2.2 and for region biomarker identification in section 3.2.3.²¹

¹⁹We used a 2006 version of HAMMER, downloaded on November 8, 2006.

²⁰Since the region-segmented version of the atlas distributed with HAMMER had much better segmentation quality than the five-segment version, as a pre-processing step we used the former to create a replacement for the latter (by simply taking the union of all the regions). The resulting five-segment atlas is dubbed ‘Atlas2’.

²¹We measured normalized region volumes. We normalized by dividing by the sum of all (98) region volumes. This sum is essentially intracranial volume minus cerebellum volume,

Each of these two HAMMER operations performs a different type of atlas-based nonlinear registration – the one that generates the RAVENS tissue maps performs less aggressive warping between the five-segment image and the atlas in order both to combat noise inherent in the registration process and to preserve volume on a tissue-by-tissue basis (so as to properly detect and encode brain atrophy). Consequently, there is considerable individual variability in RAVENS images, which we mitigate in a standard way by smoothing with a Gaussian filter with an FWHM of 5mm.

The sum of the voxel intensities over the three RAVENS maps is on the order of 10^6 and varies across individuals. Thus, prior to smoothing, we normalized each individual’s Ravens maps, such that each individual has the same total volume. However, after the normalization and smoothing (aka “nsRAVENS” images), some areas of poor registration, manifesting as areas with very low voxel values (including zero), will remain.²² For a population of nsRAVENS images, these areas are considered to be outlier areas and are thus removed from each image in the population by thresholding²³. The resulting images are the features used by our classification system.

Appendix B. Correspondence Between Atlas-defined Regions and Those Defined in (Schuff et al., 2010)

as our “intracranial region” list includes CSF in addition to brain regions and excludes the cerebellum.

²²A substantial portion of the very low, nonzero voxel intensities are in fact introduced by the smoothing itself as it calculates each new voxel intensity as a weighted average of many neighboring voxels (thereby switching some voxels from zero (non-anatomy) to very low intensity values (anatomy), which essentially slightly grows the anatomy boundaries outward).

²³We calculated the threshold solely using the *training population* of our AD-Control classifier, and then applied the thresholding operation on the entire population of AD, MCI, and Control individuals. In this way, we were careful to exclude test examples from all phases of classifier training.

Entorhinal cortex	Entorhinal cortex left/right
Fusiform gyrus	Lateral occipitotemporal gyrus right/left
Hippocampus	Hippocampal formation right/left
Inferior parietal GM	Supramarginal gyrus left/right, Angular gyrus right/left
Lateral orbitofrontal GM	Lateral front-orbital gyrus right/left
Lateral ventricles	Lateral ventricle left/right
Medial orbitofrontal GM	Medial front-orbital gyrus right/left
Parahippocampal gyrus	Parahippocampal gyrus right/left
Posterior cingulate	Cingulate region left/right
Precentral GM	Precentral gyrus right/left
Superior frontal GM	Superior frontal gyrus left/right
Superior temporal GM	Superior temporal gyrus right/left

Table B.4: Correspondence between the regions in (Schuff et al., 2010) (left) (except “Total GM” and “Total WM”) and our defined regions (right).

References

- Y. Aksu, D. J. Miller, G. Kesidis, and Q. X. Yang, “Margin-Maximizing Feature Elimination Methods for Linear and Nonlinear Kernel-Based Discriminant Functions”, *IEEE Transactions on Neural Networks*, vol. 25, no.10, pp.701-717, 2010.
- H. Braak and E. Braak, “Frequency of Stages of Alzheimer-Related Lesions in Different Age Categories”, *Neurobiology of Aging* **18**(4):351-357, July 8 1997.
- C. Chang and C. Lin, “LIBSVM : a library for support vector machines,” software available at <http://www.csie.ntu.edu.tw/~cjlin/libsvm>, 2001.
- J. M. Chambers, “Linear models”, in: *Statistical Models in S*, J. M. Chambers and T. J. Hastie (Eds.), Chapman & Hall, New York, 1993.
- D. Chan, J.C. Janssen, J.L. Whitwell, H.C. Watt, R. Jenkins, C. Frost, M.N. Rossor and N.C. Fox, “Change in rates of cerebral atrophy over time in early-onset Alzheimer’s disease: longitudinal MRI study”, *Lancet* **362**, pp. 1121-1122, 2003.
- G. Chetelat, B. Desgranges, V. de la Sayette, F. Viader, F. Eustache, J-C. Baron, “Mapping gray matter loss with voxel-based morphometry in mild cognitive impairment”, *NeuroReport* vol.13. no.15, 28 October 2002.
- Y.-Y. Chou, N. Leporé, C. Avedissian, S. K. Madsen, X. Hua, C. R. Jack Jr., M. W. Weiner, A. W. Toga, P. M. Thompson, and the Alzheimer’s

- Disease Neuroimaging Initiative, "Mapping Ventricular Expansion and its Clinical Correlates in Alzheimer's Disease and Mild Cognitive Impairment using Multi-Atlas Fluid Image Alignment", *Proc. SPIE*, vol.7259, 725930, 2009.
- Y.-Y. Chou, N. Leporé, P. Saharan, S. K. Madsen, X. Hua, C. R. Jack, L. M. Shaw, J. Q. Trojanowski, M. W. Weiner, A. W. Toga, P. M. Thompson, and the Alzheimer's Disease Neuroimaging Initiative, "Ventricular maps in 804 ADNI subjects: correlations with CSF biomarkers and clinical decline", *Neurobiology of Aging* 31, pp.1386-1400, 2010.
- J. G. Csernansky, L. Wang, J. Swank, J. P. Miller, M. Gado, D. McKeel, M. I. Miller, J. C. Morris, "Preclinical detection of Alzheimer's disease: hippocampal shape and volume predict dementia onset in the elderly", *NeuroImage* 25, pp.783-792, 2005.
- C. Davatzikos, "Mapping image data to stereotaxic spaces: Applications to brain mapping," *Hum. Brain Mapp.*, 6:334-338, 1998.
- C. Davatzikos, A. Genc, D. Xu, and S. M. Resnick, "Voxel-Based Morphometry Using the RAVENS Maps: Methods and Validation Using Simulated Longitudinal Atrophy," *NeuroImage* 14, pp.1361-1369, 2001.
- C. Davatzikos, Y. Fan, X. Wu, D. Shen, S. M. Resnick, "Detection of prodromal Alzheimer's disease via pattern classification of magnetic resonance imaging", *Neurobiology of Aging* 29, pp.514-523, 2008.
- C. Davatzikos, P. Bhatt, L. M. Shaw, K. N. Batmanghelich, J. Q. Trojanowski, "Prediction of MCI to AD conversion, via MRI, CSF biomarkers, and pattern classification", *Neurobiology of Aging*, 2010, doi:10.1016/j.neurobiolaging.2010.05.023.
- M. J. de Leon, S. DeSanti, R. Zinkowski, P. D. Mehta, D. Pratico, S. Segal, H. Rusinek, J. Li, W. Tsui, L. A. Saint Louis, C. M. Clark, C. Tarshish, Y. Li, L. Lair, E. Javier, K. Rich, P. Lesbre, L. Mosconi, B. Reisberg, M. Sadowski, J. F. DeBernadis, D. J. Kerkman, H. Hampel, L. -O. Wahlund, P. Davies, "Longitudinal CSF and MRI biomarkers improve the diagnosis of mild cognitive impairment," *Neurobiology of Aging* 27, pp.394-401, 2006.

- G. De Meyer, F. Shapiro, H. Vanderstichele, E. Vanmechelen, S. Engelborghs, P. P. De Deyn, E. Coart, O. Hansson, L. Minthon, H. Zetterberg, K. Blennow, L. Shaw, J. Q. Trojanowski, for the Alzheimers Disease Neuroimaging Initiative, "Diagnosis-Independent Alzheimer Disease Biomarker Signature in Cognitively Normal Elderly People", *Arch. Neurol.*, vol. 67, no. 8, pp.949-956, Aug 2010.
- R. Duda, P. Hart, and G. Stork, *Pattern Classification*. Second Edition, John Wiley and Sons, New York, 2001.
- Y. Fan, D. Shen, R. C. Gur, R. E. Gur, C. Davatzikos, "COMPARE: Classification of Morphological Patterns Using Adaptive Regional Elements", *IEEE Transactions on Medical Imaging*, vol. 26, no. 1, pp.93-105, 2007.
- Y. Fan, N. Batmanghelich, C. M. Clark, C. Davatzikos, "Spatial patterns of brain atrophy in MCI patients, identified via high-dimensional pattern classification, predict subsequent cognitive decline", *NeuroImage* 39, pp.1731-1743, 2008.
- C. Fennema-Notestine, D. J. Hagler Jr., L. K. McEvoy, A. S. Fleischer, E. H. Wu, D. S. Karow, A. M. Dale, the Alzheimer's Disease Neuroimaging Initiative, "Structural MRI biomarkers for preclinical and mild Alzheimer's disease", *Human Brain Mapping*, vol.30, issue 10, pp.3238-3253, 2009.
- G.B. Frisoni, A. Prestia, P.E. Rasser, M. Bonetti, P.M. Thompson, "In vivo mapping of incremental cortical atrophy from incipient to overt Alzheimer's disease", *Neurol.* **256**(6):916-24, Feb 28, 2009.
- FSL website: FSL (FMRIB Software Library), <http://www.fmrib.ox.ac.uk/fsl>
- G. Fung, O. L. Mangasarian, "A feature selection Newton method for support vector machine classification," *Computational Optimization and Applications*, vol. 28, no.2:185-202, July 2004.
- A. F. Goldszal, C. Davatzikos, D. L. Pham, M. X. H. Yan, R. N. Bryan, S. M. Resnick, "An Image-Processing System for Qualitative and Quantitative Volumetric Analysis of Brain Images," *J. Comput. Assist. Tomogr.*, 22:827-837, 1998.

- I. Guyon, J. Weston, S. Barnhill, and V. Vapnik, "Gene selection for cancer classification using support vector machines," *Machine Learning*, 46(1):389-422, 2002.
- I. Guyon and A. Elisseeff, "An introduction to variable and feature selection," *J. Mach. Learn. Res.*, vol. 3, pp.1157-1182, 2003.
- M. Jenkinson and S.M. Smith, "A global optimisation method for robust affine registration of brain images," *Med. Image Anal.*, 5(2):143-156, 2001.
- J. P. Lerch, A. C. Evans, "Cortical thickness analysis examined through power analysis and a population simulation", *NeuroImage* 24, pp.163-173, 2005.
- A. D. Leow, I. Yanovsky, N. Parikshak, X. Hua, S. Lee, A. W. Toga, C. R. Jack Jr., M. A. Bernstein, P. J. Britson, J. L. Gunter, C. P. Ward, B. Borowski, L. M. Shaw, J. Q. Trojanowski, A. S. Fleisher, D. Harvey, J. Kornak, N. Schuff, G. E. Alexander, M. W. Weiner, P. M. Thompson, Alzheimers Disease Neuroimaging Initiative. "Alzheimers Disease Neuroimaging Initiative: A One-Year Follow-up Study Using Tensor-Based Morphometry Correlating Degenerative Rates, Biomarkers and Cognition," *Neuroimage* 45, pp.645-55, 2009.
- X. -L. Meng, R. Rosenthal, D. B. Rubin, "Comparing Correlated Correlation Coefficients", *Psychological Bulletin* 111, pp.172-175, 1992.
- C. Misra, Y. Fan, C. Davatzikos, "Baseline and longitudinal patterns of brain atrophy in MCI patients, and their use in prediction of short-term conversion to AD: Results from ADNI", *NeuroImage* 44, pp.1415-1422, 2009.
- R. C. Petersen, *Mild cognitive impairment: aging to Alzheimer's Disease*, Oxford University Press, 2004.
- H. Rusinek, Y. Endo, S. De Santi, D. Frid, W.-H. Tsui, S. Segal, A. Convit, "Atrophy rate in medial temporal lobe during progression of Alzheimer's disease", *Neurology*, vol.63, issue 12, 2354-2359, 2004.
- J. M. Schott, S. L. Price, C. Frost, J. L. Whitwell, et al, "Measuring atrophy on Alzheimer disease - A serial MRI study over 6 and 12 months," *Neurology*, 65(1), pp.119-124, 2005.

- N. Schuff, D. Tosun, P. S. Insel, G. C. Chiang, D. Truran, P. S. Aisen, C. R. Jack, Jr., M. W. Weiner, the Alzheimer's Disease Initiative, "Nonlinear time course of brain volume loss in cognitively normal and impaired elders", *Neurobiology of Aging*, 2010, doi:10.1016/j.neurobiolaging.2010.07.012.
- S. M. Smith, "Fast robust automated brain extraction," *Human Brain Mapping*, 17(3):143-155, 2002.
- D. Shen and C. Davatzikos, "HAMMER: hierarchical attribute matching mechanism for elastic registration," *IEEE Trans. Medical Imaging*, 21(11):1421-1439, 2002.
- D. Shen, C. Davatzikos, "Very High-resolution Morphometry Using Mass-preserving Deformations and HAMMER Elastic Registration," *NeuroImage* 18, pp.28-41, 2003.
- SPM website: Statistical Parametric Mapping (SPM), <http://www.fil.ion.ucl.ac.uk/spm>
- T. R. Stoub, M. Bulgakova, S. Leurgans, D. A. Bennett, D. Fleischman, D. A. Turner, L. deToledo-Morrell, "MRI predictors of risk of incident Alzheimer disease," *Neurology* 64, pp. 1520-1524, 2005.
- P. M. Thompson, K. M. Hayashi, G. de Zubicaray, A. L. Janke, S. E. Rose, et al, "Dynamics of gray matter loss in Alzheimer's disease," *J. Neurosci.* 23, pp.994-1005, 2003.
- V. Vapnik, *Statistical Learning Theory*. John Wiley & Sons, 1998.
- P. Vemuri, J. L. Gunter, M. L. Senjem, J. L. Whitwell, K. Kantarci, D. S. Knopman, B. F. Boeve, R. C. Petersen, C. R. Jack Jr., "Alzheimer's disease diagnosis in individual subjects using structural MR images: Validation studies," *NeuroImage* 39, pp.1186-1197, 2008.
- P. Vemuri, H. J. Wiste, S. D. Weigand, L. M. Shaw, J. Q. Trojanowski, M. W. Weiner, D. S. Knopman, R. C. Petersen, C. R. Jack Jr., and On behalf of the Alzheimer's Disease Neuroimaging Initiative, "MRI and CSF biomarkers in normal, MCI, and AD subjects: Predicting future clinical change," *Neurology* 73:294-301, 2009.

- Y. Wang, Y. Fan, P. Bhatt, C. Davatzikos, “High-dimensional pattern regression using machine learning: From medical images to continuous clinical variables,” *NeuroImage* 50, pp.1519-1535, 2010.
- Y. Zhang, M. Brady, and S. Smith, “Segmentation of brain MR images through a hidden Markov random field model and the expectation maximization algorithm,” *IEEE Trans. Medical Imaging*, 20(1):45-57, 2001.
- D. Zhang, Y. Wang, L. Zhou, H. Yuan, D. Shen, and the Alzheimer’s Disease Neuroimaging Initiative, “Multimodal classification of Alzheimer’s disease and mild cognitive impairment,” *NeuroImage*, 2011, doi:10.1016/j.neuroimage.2011.01.008.